

The circumstellar CO emission of RV Bootis

Evidence for a Keplerian disk?

P. Bergman¹, F. Kerschbaum^{2,3}, and H. Olofsson³

¹ Onsala Space Observatory, 439 92 Onsala, Sweden

² Institut für Astronomie, Türkenschanzstrasse 17, 1180 Wien, Austria

³ Stockholms Observatorium, 133 36 Saltsjöbaden, Sweden

Received 27 August 1999 / Accepted 26 October 1999

Abstract. We report on high-resolution CO $J=1-0$ and $J=2-1$ interferometric observations of the oxygen-rich semiregular variable RV Boo supplemented by single-dish multi-transition data of CO($J=1-0$, $2-1$, $3-2$, $4-3$). Detections of the thermal SiO($v=0$, $J=2-1$, $3-2$) transitions as well as the vibrationally excited SiO($v=1$, $J=2-1$) line are also reported. The interferometric CO $J=2-1$ observations, with a spatial resolution of about $1''.7$, reveal a disk-like structure of size $4''.2 \times 3''.3$ around RV Boo. Furthermore, the position-velocity information along a line through the center of the source at a position angle of about 150° can be interpreted as a sign of Keplerian rotation. Six symmetrically placed features, possibly corresponding to three rings, around a central feature are seen. These observations may therefore, to our knowledge, present the first indications of a rotating disk around an AGB star. However, it cannot be fully excluded that the observed kinematical structure is caused by a bipolar outflow. From the single-dish CO observations we estimate the molecular mass of the source to be $3 \times 10^{-5} M_\odot$.

Key words: stars: variables: general – stars: AGB and post-AGB – stars: circumstellar matter – stars: mass-loss – radio lines: stars

1. Introduction

The presence of extensive stellar mass loss on the asymptotic giant branch (AGB) is well established. It starts early on the AGB, and very likely increases as the star evolves, reaching its maximum at the end before a planetary nebula is formed. Probably, the higher-mass stars reach higher terminal mass loss rates, the so called super-wind phase, and there is also very likely a dependence on metallicity (Habing 1996). However, the details are less known, e.g., the geometry, which is the subject of this paper, and the small-scale density distribution. Information on the geometry of the AGB mass loss was first obtained from interferometry maps of OH 1612 MHz maser emission (Booth et al. 1981; Bowers & Johnston 1990). These, as well as CO radio line maps of the carbon star IRC+10216 (Truong-Bach et al.

1991), were consistent with an over-all spherically symmetric mass loss. Recent CO radio line interferometric maps of a large number of AGB-stars are also consistent with this (Neri et al. 1998; considering the limited S/N-ratio), and in particular the detached CO shells of a few carbon stars appear to be very close to spherical (Olofsson et al. 1996, 1998, 1999). Opposite views have been given, e.g., by Stanek et al. (1995) based on single-dish CO($3-2$) maps, but the spatial resolution as well as the S/N-ratios are limited.

However, there are also indications that the situation is more complicated than this. For instance, Margulis et al. (1990) noted that a large fraction of the CO line profiles obtained towards O-rich AGB-stars deviated significantly from that expected from a spherical envelope. For two objects there is also clear evidence for a more complicated spatial structure, V Hya (semiregular carbon star; Kahane et al. 1996) and X Her (semiregular O-rich star; Kahane & Jura 1996). Furthermore, Knapp et al. (1998) found evidence for multiple winds with different expansion velocities. This was corroborated by Kerschbaum & Olofsson (1999) in a study where they identified a small group of O-rich semiregular and irregular variables, EP Aqr, RV Boo, X Her, and SV Psc (all are SRBs), that clearly show multi-component line profiles: typically a very narrow feature with a full width less than $\sim 5 \text{ km s}^{-1}$ is centered, within the uncertainties, on a much broader line $\sim 18 \text{ km s}^{-1}$. The broad component is close to being parabolic. The central peaks are very narrow, and, if interpreted as arising from expanding envelopes, they imply expansion velocities of $\sim 2 \text{ km s}^{-1}$.

One possible interpretation of such observations is outlined in Kahane & Jura (1996) where they report on a bipolar outflow around X Her. They were able to spatially resolve the blue- and red-shifted sides of the broad component, and inferred a (weakly collimated) bipolar outflow, while the low-velocity emission, i.e., the narrow component, appears to outline a symmetric envelope. Knapp et al. (1998), on the other hand, suggest a scenario where episodic mass-loss plays a rôle. A similar narrow spike in the middle of a broader line could also be interpreted in terms of emission from a long-lived disk as suggested by Jura et al. (1995) for the post-AGB object the Red Rectangle, and by Kahane et al. (1998) for the “silicate” carbon star BM Gem.

Send offprint requests to: P. Bergman (bergman@oso.chalmers.se)

Table 1. Single-dish line measurements

Line	Telescope	HPBW (")	I (K km s ⁻¹)	T_{mb} (K)	v_{LSR} (km s ⁻¹)	v_e (km s ⁻¹)	Note
SiO($J=3-2$, $v=0$)	IRAM	19	2.50	0.25	8.6:	8.0:	
SiO($J=2-1$, $v=0$)	OSO	44	1.11	0.12	9.4	7.2	
SiO($J=2-1$, $v=1$)	OSO	44	0.60	0.14	7.7		
CO($J=4-3$)	JCMT	11	8.87	1.11	10.2:	6.2:	
CO($J=3-2$)	JCMT	13	6.81	0.86	7.4	7.5	
			2.13	0.38	8.4	2.8	narrow
			5.00	0.52	7.6	8.4	broad
CO($J=2-1$)	JCMT	21	4.47	0.51	7.9	7.8	
			0.84	0.19	8.3	2.7	narrow
			3.65	0.32	8.0	8.1	broad
CO($J=1-0$)	IRAM	22	3.21	0.33	7.9	8.1	

Finally, one should note the well-known fact that deviations from spherical symmetry seem to be common if not the rule for planetary nebulae. Somehow, this asymmetry must be related to the properties of the AGB envelope. The evidence presently favour that the AGB wind becomes axi-symmetric at the very last stages of the AGB evolution, and that the interaction with a fast wind from the post-AGB object further enhances the axi-symmetry.

In this paper we will present and discuss CO radio line observations, performed with the OVRO mm-wave interferometer, of RV Boo, one of the sources with multi-component CO line profiles, together with additional single-dish, multi-transition CO and SiO radio line data.

2. The semiregular variable RV Boo

The semiregular variables (SRVs; types SRa and SRb) are a quite numerous group of objects among the stars on the AGB. In a series of papers they have been studied in a broad and systematic way (Kerschbaum & Hron 1992, 1994, 1996; Kerschbaum 1995; Kerschbaum et al. 1996).

RV Boo (IRC+30261, IRAS14371+3245, HIP71644) is an O-rich SRV of type SRb with a GCVS-period of $\sim 140^{\text{d}}$ and an amplitude in Johnson B of close to 2 magnitudes. Lebzelter (1999) found a radial-velocity amplitude of $\sim 4 \text{ km s}^{-1}$, from NIR ro-vibrational transitions of CO, which is typical for this variability type. The associated period is roughly 120^{d} . Photometric data from the same group confirm this timescale of variation, but also indicate a more complex lightcurve with variable amplitudes and a changing mean light level.

Its spectral class varies between M5III and M7III with indications of emission lines, which is not common among SRb variables (Kerschbaum & Hron 1992). Since RV Boo is not present in the IUE, ROSAT, or HST archives any chromospheric activity is unknown. Little et al. (1987) found no, or only marginal, indications of technetium in its spectrum, and hence there is no apparent evidence for a recent thermal pulse. Its IRAS-colours are similar to that of a red Mira-variable [region IIIa in the van der Veen & Habing (1988) diagramme]. In the classification system by Kerschbaum & Hron (1992) it is a “red” SRV.

The Hipparcos parallax puts RV Boo at a distance of 390 pc with a formal $\pm 1\sigma$ range of 280 to 640 pc. Integrating its spectral energy distribution from the visual to the far infrared leads to a luminosity of $8100 L_{\odot}$ ($4200\text{--}21400 L_{\odot}$, respectively). This seems to be somewhat high when compared to typical O-rich SRVs (Kerschbaum et al. 1997).

From CO radio line observations the mass loss rate of RV Boo was estimated to be $\sim 2 \times 10^{-7} M_{\odot} \text{ yr}^{-1}$ by Kahane & Jura (1994). However, they noted the strange CO line profiles which did not allow a good fit of their model. Kerschbaum et al. (1997), using independent measurements, arrived at $\sim 4 \times 10^{-8} M_{\odot} \text{ yr}^{-1}$. Kerschbaum & Olofsson (1999) assigned RV Boo to a group of objects with multi-component CO radio line spectra. RV Boo was included in a number of maser-surveys but was never detected [e.g., Spencer et al. (1981) searched for SiO, Lewis (1997) for H₂O, te Lintel Hekkert et al. (1991) for OH].

The spectral energy distribution of RV Boo, as deduced from near-IR and IRAS photometry, indicates a significant contribution by circumstellar dust, and it can be, to first order, approximated by a combination of two blackbodies of ~ 2800 and ~ 450 K (cf. Kerschbaum & Hron 1996). Its dust mass loss rate was estimated to be about $2 \times 10^{-10} M_{\odot} \text{ yr}^{-1}$ from the IRAS $60 \mu\text{m}$ flux (Kerschbaum et al. 1996), which suggests a gas-to-dust mass ratio of a few hundred. Young et al. (1993a, 1993b) found no indications of extended emission in their analysis of the IRAS data. The IRAS-LRS class is 22, i.e., weak silicate emission.

A comparison of a low resolution archive ISO-SWS spectrum of RV Boo (GT programme *sprice: startyp1*) with typical ones of O-rich semiregulars (OT programmes *fkerschb: orich-srv/orichsrl/zzagb2pn*) does not indicate deviating properties. The emission of the ν_3 ro-vibrational band of SO₂ at about $7.3 \mu\text{m}$ and of the Q -branch ro-vibrational transitions of CO₂ around $15 \mu\text{m}$ may indicate the presence of a warm molecular layer at a distance of a few stellar radii from the star (cf. Justtanont et al. 1998; Yamamura et al. 1999). There are also emission features of amorphous silicates around 10 and $18 \mu\text{m}$, as well as a prominent $13 \mu\text{m}$ feature, which is quite typical for low mass loss rate, O-rich AGB stars (e.g., Kerschbaum et

al. 1997). It is frequently attributed to corundum (crystalline Al_2O_3 ; e.g., Begemann et al. 1997). An alternative identification of the $13\ \mu\text{m}$ feature in terms of MgAl_2O_4 (spinel) was presented recently (Posch et al. 1999). No evidence is found for the presence of crystalline forms of silicates.

Taken together, neglecting its strange CO radio line profiles, RV Boo seems to be a quite normal low mass loss rate, semiregular variable.

3. Observations

3.1. Single-dish data

New observations in the SiO ($v=0, J=2-1$) and SiO ($v=1, J=2-1$) lines were obtained using the radome enclosed 20 m telescope at Onsala Space Observatory¹ (OSO), Sweden. The OSO data were collected in April and June 1999. The main beam efficiency of the telescope was 0.55, and the representative noise temperature of the receiver was 150 K. The beam size is $44''$ at 86 GHz. As spectrometers two filterbanks were used (256×250 kHz and 512×1 MHz). Dual beam switching (beam separation of about $11'$), in which the source was placed alternately in the two beams, was used to eliminate baseline ripples. All data were calibrated by the chopper-wheel method. The CO ($J=2-1, 3-2, 4-3$) data were taken from Kerschbaum & Olofsson (1999). The SiO ($v=0, J=3-2$) and CO ($J=1-0$) spectra, obtained with the IRAM 30 m telescope, were kindly provided by Martin Groenewegen. Fig. 1 shows all our single-dish spectra. The intensity scale is given in terms of main beam brightness temperature, T_{mb} . Table 1 lists the corresponding line measurements. The tabulated integrated line intensity, I , is given in main beam brightness temperature scale and the beam size is given as the half power beam width (HPBW). The peak temperature (T_{mb}), the centre velocity (v_{LSR}), and the expansion velocity (v_e) were obtained by fitting a parabola to the line profile. In order to convert the given v_{LSR} values into the heliocentric frame $14.6\ \text{km s}^{-1}$ has to be subtracted. The note in the last column indicates if the broad or narrow components were measured separately.

All line profiles (except the non-thermal $v=1$ SiO line profile) in Fig. 1 look similar, i.e., they show a narrow central peak surrounded by weaker red- and blue-shifted shoulders. Moreover, for the CO data there is a tendency that the central peak becomes more pronounced relative to the shoulders the higher the frequency of the transition.

3.2. Interferometric observations and results

We have made high spatial resolution CO ($J=1-0$ and $2-1$) observations of RV Boo using the Owens Valley Radio Observatory (OVRO) six-element array. The observations were made in December 1997 and January 1998 in two different telescope configurations with baselines in the range 15–119 m.

¹ The Onsala 20 m telescope is operated by the Swedish National Facility for Radio Astronomy, Onsala Space Observatory, at Chalmers University of Technology

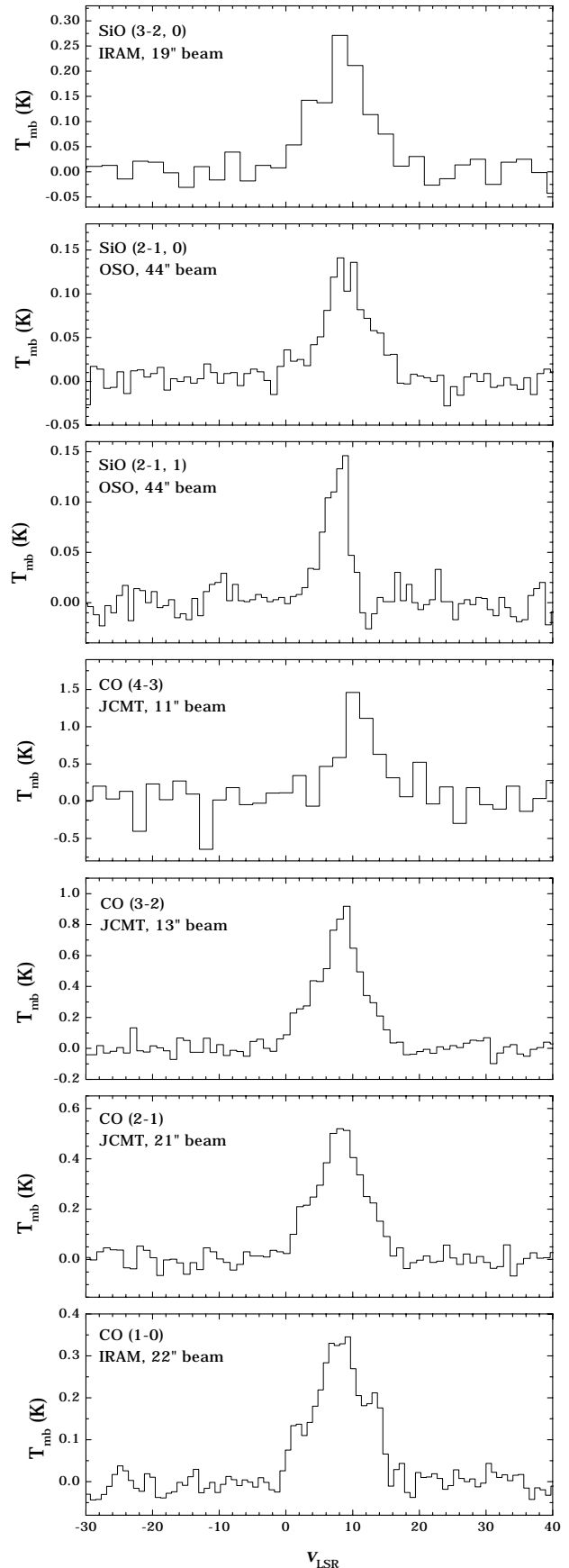


Fig. 1. Single-dish SiO and CO radio line spectra of RV Boo

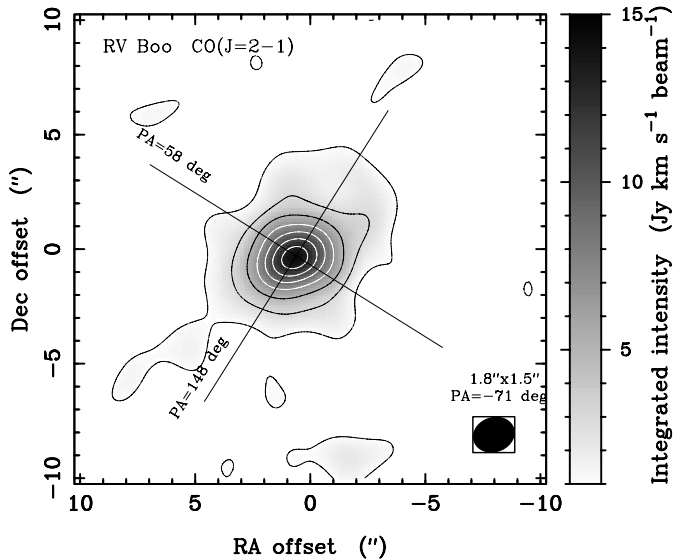


Fig. 2. CO map of the integrated intensity in the $J=2-1$ transition at 230 GHz. The size of the synthesised beam is indicated in the lower right corner. The first contour corresponds to $1 \text{ Jy km s}^{-1} \text{ beam}^{-1}$ and the increment between contours is $2 \text{ Jy km s}^{-1} \text{ beam}^{-1}$. The measured noise in the map is $0.63 \text{ Jy km s}^{-1} \text{ beam}^{-1}$. The lines denote the two ‘cuts’ used for the diagrams in Fig. 5

A digital correlator configured with 64 channels provided a spectral resolution of 0.5 MHz (or 1.3 km s^{-1} at 115 GHz , and 0.65 km s^{-1} at 230 GHz). Absolute flux calibration was obtained by measurements of Neptune and Uranus. The nearby quasar 1611+343 was used to monitor phase and gain variations. The flux densities of 1611+343 during the time of observations were measured to be 2.3 Jy at 115 GHz and 1.1 Jy at 230 GHz . The instrumental passband responses were derived by observing the bright quasar 3C273. Phase, passband, and flux calibration was carried out using the Caltech MMA data reduction package (Scoville et al. 1993). After the uv data had been calibrated and the tracks combined into two single datasets spectral line maps were made using the CLEAN algorithm in the NRAO AIPS package. The resulting synthesised beams (using uniform weighting of the uv data) are $1''.8 \times 1''.5$ ($\text{PA} = -71^\circ$) and $3''.8 \times 3''.1$ ($\text{PA} = -67^\circ$) at 230 GHz and 115 GHz , respectively.

A map of the total integrated intensity of the $J=2-1$ line is shown in Fig. 2. The map is centred at $\alpha(1950) = 14^{\text{h}}37^{\text{m}}09^{\text{s}}.29$ and $\delta(1950) = 32^\circ45'15''.2$. By fitting an elliptical Gaussian to the structure we find a source size of $4''.2 \times 3''.3$ ($\text{PA} = 123^\circ$) centred at the offsets $(0''.6, -0''.3)$. The measured offsets are consistent with the expected proper motion of RV Boo since 1950 which amounts to $(0''.7, -0''.2)$. The positional uncertainties are estimated to be $0''.2$. As can be seen in Fig. 2 the source is clearly resolved with our $J=2-1$ beam. It is marginally resolved at 115 GHz , and therefore we will mainly use the $J=2-1$ data in the analysis (the signal-to-noise ratio is also higher in the 230 GHz data).

To compare the total flux density of the $J=2-1$ interferometer map with that of the $J=2-1$ single-dish spectrum we

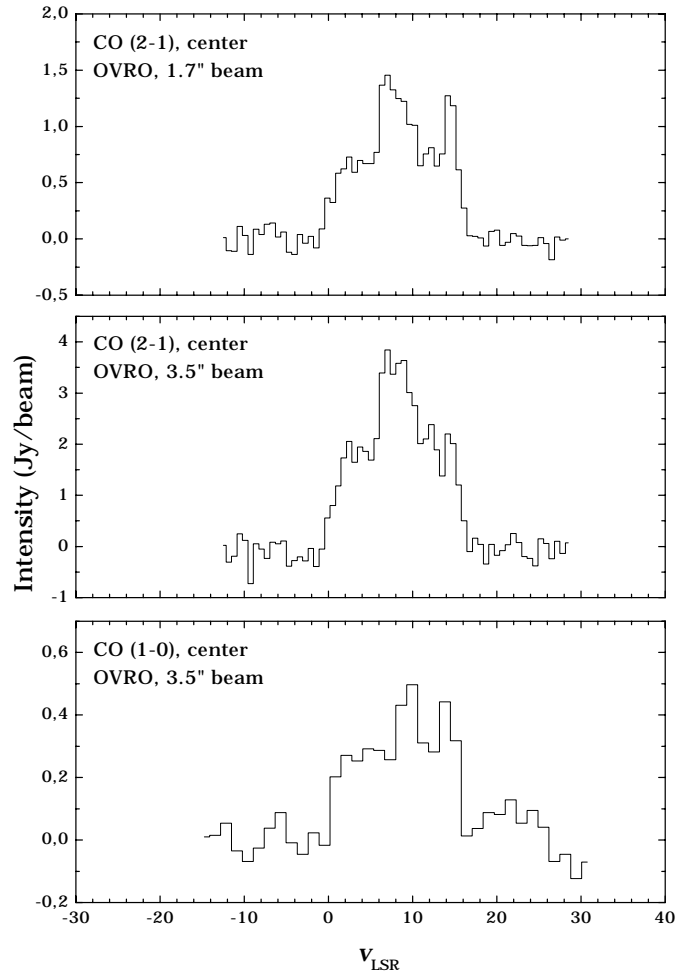


Fig. 3. CO $J=2-1$ (top) and $J=1-0$ (bottom) spectra at the kinematical centre of RV Boo. The middle $J=2-1$ spectrum has been convolved with the beam size at 115 GHz

have convolved the interferometric spectra with a $21''$ Gaussian beam. Toward the centre position we obtain an integrated flux density of $81 \pm 5 \text{ Jy km s}^{-1}$ in the $21''$ beam. The JCMT single-dish spectrum yields an integrated flux density of 79 Jy km s^{-1} (using a conversion factor of 17.6 Jy K^{-1} valid for conversion between flux density and the T_{mb} -scale in the case of a small source). This implies that, within the calibration uncertainties, we observe all flux in the interferometer maps. In Fig. 3 we display the $J=1-0$ and $J=2-1$ spectra at the centre of the source. Also displayed is the $J=2-1$ spectrum as convolved with the $J=1-0$ beam.

The $J=2-1$ channel maps clearly show that the CO source structure varies with velocity, see Fig. 4. The position shift is most evident when comparing the maps at 7.0 km s^{-1} and 9.6 km s^{-1} . To find the symmetry axis we made several cuts (of length $15''$), at different position angles through the centre offsets $(0''.6, -0''.3)$, along which we determined the position-velocity structure. Along a cut with position angle of 58° the structure becomes almost symmetric with respect to the emission centre, see the upper diagramme in Fig. 5. The lower diagramme in Fig. 5 shows the position-velocity structure along a

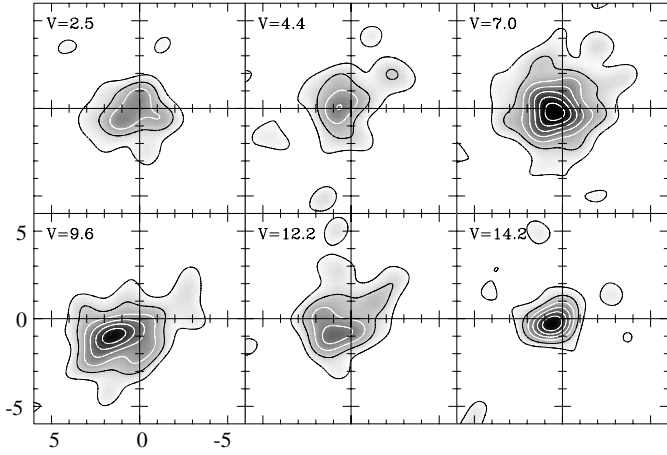


Fig. 4. Selected CO $J=2-1$ channel maps. The channel velocity is indicated in the upper left corner of each panel. The first contour corresponds to 0.2 Jy beam^{-1} and the contour increment is 0.2 Jy beam^{-1} . The offsets are given in arcseconds and RV Boo is located at $(0''.7, -0''.2)$

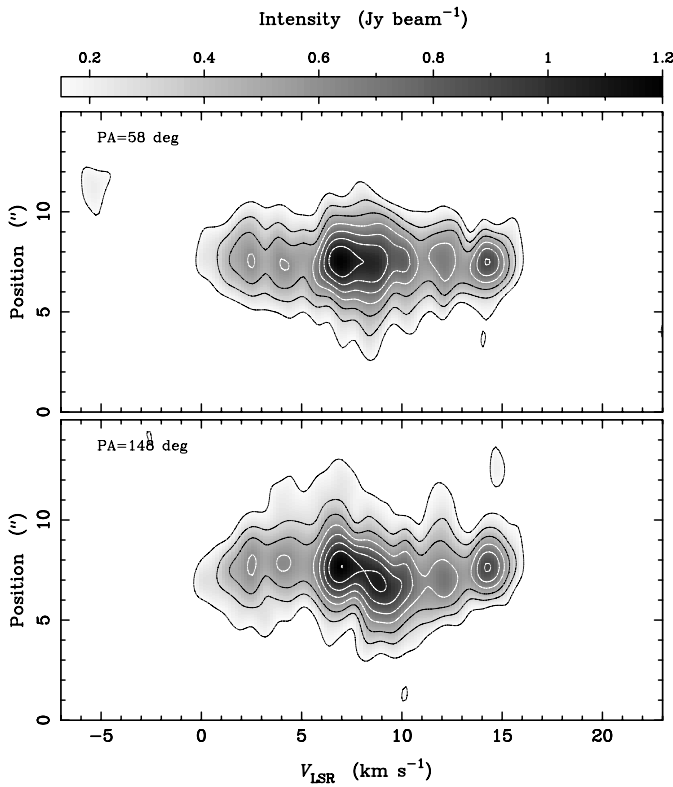


Fig. 5. Position-velocity diagrammes along the two axes indicated in Fig. 2. The first contour corresponds to $0.15 \text{ Jy beam}^{-1}$ and the contour increment is $0.15 \text{ Jy beam}^{-1}$. Increasing position value corresponds to decreasing RA offset in Fig. 2

line (at $\text{PA} = 148^\circ$) perpendicular to the symmetric cut. Here we see a systematic variation of source structure as a function of velocity. We note also that the lower contours of the $J=2-1$ brightness distribution (which are less affected by the beam) appear to have a symmetry axis of $\text{PA} \sim 150^\circ$.

3.3. Physical conditions

Using the estimated source size ($4''.2 \times 3''.3$) obtained from the $J=2-1$ interferometer map and the mean intensity ($\sim 0.3 \text{ K}$) of the $\text{CO}(J=2-1)$ single-dish line profile, we obtain a lower limit of 15 K to the average excitation temperature in the $J=2-1$ transition. This lower limit of 15 K can also be taken as a lower limit on the average kinetic temperature of the source (unless severe non-LTE effects are at work).

Since the exact nature of the emission around RV Boo is unknown (it is definitely not a ‘normal’ spherical envelope) we will crudely estimate the physical parameters by modelling the observed line ratios under the assumption of a large velocity gradient (LVG). We adopt a CO abundance with respect to H_2 of $f_{\text{CO}} = 2 \times 10^{-4}$ (see Kahane & Jura 1994). The velocity gradient, dv/dr , is simply calculated as the line width divided by the source size, $\sim 10^3 \text{ km s}^{-1} \text{ pc}^{-1}$.

Using the integrated intensities in Table 1 (corrected for beam filling) the CO line ratios become: 1.3, 0.61, and 0.96 for the $2-1/1-0$, $3-2/2-1$, and $4-3/3-2$ ratios, respectively. Here the $4-3/3-2$ ratio is rather uncertain due to the low S/N ratio of the $J=4-3$ spectrum. The LVG modelling of the CO line ratios points at a kinetic temperature larger than 25 K (in line with the lower limit of 15 K found previously), and an H_2 density in the range $10^{3.2} - 10^{3.8} \text{ cm}^{-3}$. Under these circumstances we were able to fit the $2-1/1-0$ and $3-2/2-1$ ratios reasonably well whilst the modelled $4-3/3-2$ ratio is a factor of about two lower than the measured ratio. This could be a result of the poor S/N ratio in the $J=4-3$ spectrum. Also, since we here assumed a homogeneous model source the possibility that the central feature is more pronounced in the $J=4-3$ spectrum (see Fig. 1), may have an effect. The best fit was obtained when the velocity gradient was set to $250 \text{ km s}^{-1} \text{ pc}^{-1}$ (a factor of four lower than estimated above), i.e., using $f_{\text{CO}}/(dv/dr) = 8 \times 10^{-7} (\text{km s}^{-1} \text{ pc}^{-1})^{-1}$. Moreover, we find that the observed $v=0$ SiO $3-2/2-1$ line ratio of 0.43 is consistent with H_2 densities less than 10^4 cm^{-3} at higher kinetic temperatures ($T_k \geq 25 \text{ K}$) and for a reasonable SiO abundance of a few $\times 10^{-7}$. Since the line profiles of CO and thermal SiO look similar (see Fig. 1) we conclude that it is plausible that most of the emission from CO and thermal SiO arises from the same source.

If we adopt an H_2 density of $3 \times 10^3 \text{ cm}^{-3}$ we arrive at a total mass of $3 \times 10^{-5} M_\odot$ for the CO line-emitting gas.

4. Interpretation

The single-dish CO line profiles are reasonably described as consisting of two components: a broad ($\sim 16 \text{ km s}^{-1}$) symmetric (except for the $J=1-0$ line, where the red-shifted side is stronger) component, with a much narrower ($\sim 6 \text{ km s}^{-1}$) component, centered on the broad one, that becomes more prominent the higher the transition, Fig. 1. The latter must be an effect of increased excitation requirements since the source is smaller than $\sim 4''$. The $v=0$ SiO spectra to a large degree resemble the CO spectra, perhaps with a tendency for the broad component to be stronger on the red-shifted side of the higher S/N-ratio $J=2-1$ spectrum. We managed to detect a weak and relatively

narrow (a Gaussian fit gives a full width at half maximum of 4.2 km s^{-1}) SiO($v=1, J=2-1$) maser feature (to our knowledge the first detection of maser emission from this star), which is centred at $\sim 7.7 \text{ km s}^{-1}$ (roughly the centre velocity of all other lines, see Table 1). The interferometer CO spectra more clearly separate these two components, and in the $J=2-1$ spectrum a new, narrow feature on the extreme red-shifted side appears, Fig. 3. The latter appears to be spatially unresolved, since it is less prominent in the “convolved” $J=2-1$ spectrum, and more prominent in the $J=1-0$ line (cf. the single-dish spectra). A more careful examination of the $J=2-1$ data reveals the presence of seven features, six features are symmetrically placed ($\pm 1.5, \pm 4$, and $\pm 6 \text{ km s}^{-1}$) around a central feature at $\sim 8.3 \text{ km s}^{-1}$. These features are clearly seen in the upper panel of Fig. 5, and also, although less evident, in the $J=1-0$ data (not shown here). The velocities of the six channel maps in Fig. 4 correspond to the velocities of these six features. The central feature is very narrow ($\sim 2 \text{ km s}^{-1}$) and becomes more prominent when only the highest spatial resolution interferometer data are used. Thus, it is unresolved and it is very likely coming from a higher-excitation region, i.e., it is the feature that becomes more prominent in the higher transition single-dish spectra. The $\pm 1.5 \text{ km s}^{-1}$ features are spatially dislocated, as is shown in the lower panel of Fig. 5. This may point in the direction of a bipolar outflow (cf. Kahane & Jura 1996), but there is additional kinematical structure. In order to quantify this we fitted a Gaussian in each velocity channel of the data in the lower panel of Fig. 5. The centre positions of these Gaussians, relative to the emission centre, are displayed as filled circles in Fig. 6. The results for the $J=1-0$ data are shown with crosses. There is clearly a systematic variation in the line-of-sight velocity, even though it occurs on a scale smaller than the beam. Starting at the extreme red- and blue-shifted velocities in the $J=2-1$ data the emission regions, symmetrically placed in velocity with respect to the line centre, becomes more and more (symmetrically) displaced, with respect to the emission centre, along $\text{PA} \sim 150^\circ$ as the line centre is approached. This kinematical structure is very reminiscent of Keplerian rotation, and in Fig. 6 we have drawn lines corresponding to a Keplerian rotation curve with a central mass of $1.5 M_\odot$. The similarity between the measured velocities and the Kepler curve around an object with a mass roughly expected for RV Boo (its high luminosity may point to an even higher mass) is striking, and an interpretation in the form of a low-mass disk, seen close to edge-on, surrounding RV Boo is tempting. We cannot at this point explain the presence of distinct features in the emission. In the case of a disk they (except for the central feature) would seem to correspond to material being accumulated into three rings. In fact, a model consisting of three rings (or sub-disks) with radii 20–35, 55–85, and 300–450 AU mimics the observed features quite nicely. To our knowledge, these observations present the first indications of a rotating disk around an AGB star.

The central feature, apparently originating in an unresolved high-excitation region, is difficult to interpret. It appears not to move systematically (along the line-of-sight) with respect to the disk emission. It could possibly be attributed to a low-velocity ($v_e \sim 2 \text{ km s}^{-1}$) spherical wind close to the star. It

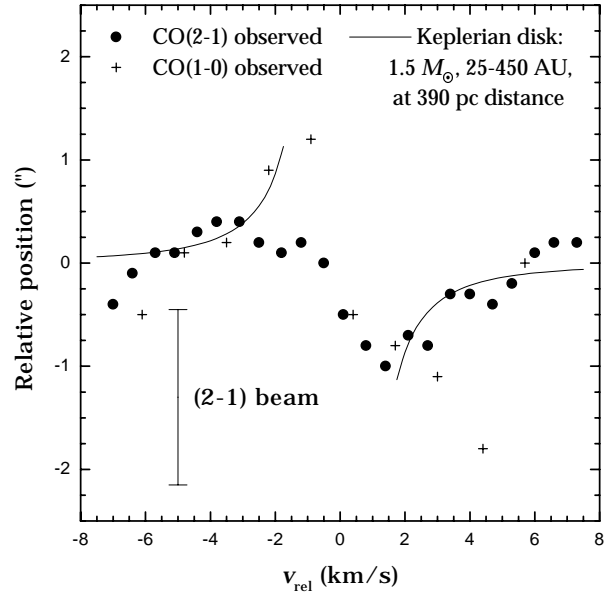


Fig. 6. The velocity structure of the circumstellar CO emission from RV Boo. Filled circles are the $J=2-1$ points and crosses indicate the $J=1-0$ points (see text for details). Plotted is also a Keplerian rotation curve for a central mass of $1.5 M_\odot$.

resembles closely the very narrow features seen towards EP Aqr and SV Psc (Kerschbaum & Olofsson 1999).

5. Outlook

It appears that among the low mass-loss rate AGB-stars there is a higher frequency of peculiar circumstellar CO line profiles. This may suggest that the morphology of their circumstellar envelopes is more complex than that of higher mass loss rate objects, although in the latter case the emission may not probe well the density distribution due to saturation effects. In any case, spatial information is of particular importance here in order to reach a better understanding of the AGB mass loss process. The most nearby objects can be mapped in suitable molecular emissions and with enough spatial resolutions with mm-wave interferometers. In the case of RV Boo, higher spatial resolution data than presented here are required to convincingly reveal the structure of its circumstellar envelope.

Acknowledgements. The authors are grateful to the referee C. Kahane for constructive comments on the manuscript and Martin Groenewegen for providing them with valuable IRAM observations. PB and HO acknowledge financial support from the Swedish Natural Science Research Council (NFR). The work of FK was supported by APART (Austrian Programme for Advanced Research and Technology) from the Austrian Academy of Sciences. FK was also supported by the Österreichische Nationalbank under the Jubiläumsfonds-project number 6876. This research has made use of the SIMBAD database.

References

- Begemann B., Dorschner J., Henning Th., et al., 1997, *ApJ* 476, 199
Booth R.S., Norris R.P., Porter N.D., Kus A.J., 1981, *Nat* 290, 382

- Bowers P.F., Johnston K.J., 1990, ApJ 354, 676
Habing H.J., 1996, A&AR 7, 97
Jura M., Balm S.P., Kahane C., 1995, ApJ 453, 721
Justtanont K., Feuchtgruber H., de Jong T., et al., 1998, A&A 330, L17
Kahane C., Jura M., 1994, A&A 290, 183
Kahane C., Jura M., 1996, A&A 310, 952
Kahane C., Audinos P., Barnbaum C., Morris M., 1996, A&A 314, 871
Kahane C., Barnbaum C., Uchida K., Balm S.P., Jura M., 1998, ApJ 500, 466
Kerschbaum F., 1995, A&AS 113, 441
Kerschbaum F., Hron J., 1992, A&A 263, 97
Kerschbaum F., Hron J., 1994, A&AS 106, 397
Kerschbaum F., Hron J., 1996, A&A 308, 489
Kerschbaum F., Olofsson H., 1999, A&AS 138, 299
Kerschbaum F., Olofsson H., Hron J., 1996, A&A 311, 273
Kerschbaum F., Olofsson H., Hron J., 1997, In: Sasselov D.D., Takeuti M. (eds.) Proc. of JD24, 23rd GA of the IAU, 17.–30.8.1997, Kyoto, Japan, Universal Academy Press Inc., Tokyo, Japan, p. 177
Knapp G.R., Young K., Lee E., Jorissen A., 1998, ApJS 117, 209
Lewis B.M., 1997, AJ 114, 1602
Lebzelter T., 1999, A&A, in press
Little S.J., Little-Marenin I.R., Bauer W.H., 1987, AJ 94, 981
Margulis M., van Blerkom D.J., Snell R.L., Kleinmann S.G., 1990, ApJ 361, 673
Neri R., Kahane C., Lucas R., Bujarrabal V., Loup C., 1998, A&AS 130, 1
Olofsson H., Bergman P., Eriksson K., Gustafsson B., 1996, A&A 311, 587
Olofsson H., Bergman P., Lucas R., et al., 1998, A&A 330, L10
Olofsson H., Bergman P., Lucas R., et al., 1999, A&A, in press
Posch T., Kerschbaum F., Mutschke H., et al., 1999, A&A, in press
Scoville N.Z., Carlstrom J.E., Chandler C.J., et al., 1993, PASP 105, 1482
Spencer J.H., Winnberg A., Olsson F.M., et al., 1981, AJ 86, 392
Stanek K.Z., Knapp G.R., Young K., Phillips, T.G., 1995, ApJS 100, 169
te Lintel Hekkert P., Caswell J.L., Habing H.J., Haynes R.F., Norris R.P., 1991, A&AS 90, 327
Truong-Bach, Morris D., Nguyen-Q-Rieu, 1991, A&A 249, 435
van der Veen W.E.C.J., Habing H., 1988, A&A 194, 125
Yamamura I., de Jong T., Onaka T., Cami J., Waters L.B.F.M., 1999, A&A 341, L9
Young K., Phillips T.G., Knapp G.R., 1993a, ApJS 86, 517
Young K., Phillips T.G., Knapp G.R., 1993b, ApJ 409, 725